Electronic Supplementary Material (ESI) for Journal of Materials Chemistry C.

Supplementary Information

Vertical CNT-Ecoflex Nanofins for Highly Linear Broad-Range-Detection Wearable Strain Sensor

Shuo Zhang, Lei Wen, Huan Wang, Kai Zhu and Min Zhang*

School of Electronic and Computer Engineering, Peking University, Shenzhen 518055, China.

***E-mail: zhangm@ece.pku.edu.cn**

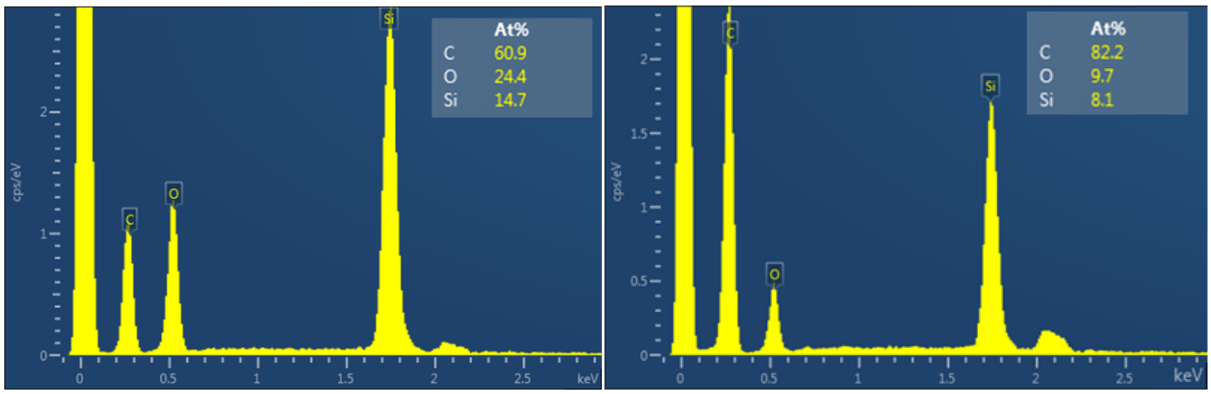

Fig. S1 The Energy Dispersive Spectrometer of the (a) CNT-Ecoflex Nanofins and (b) PDMS transferred vertical CNT networks. Both the images demonstrate that no Fe catalysis remains on the microstructures formed after the transfer. Besides, the vertical CNT network has high carbon atom percentage than that in the Nanofins, since the CNTs in the Nanofins are covered by Ecoflex, while the vertical CNT network is exposed outside.

Table S1. Summary of the performance of the stretchable strain sensor reported up to now.[1-16]

Active materials	Sensing mechanism	Minimum detection	Maximum detection	Sensitivity (gauge factor)		Linearity (R^2)	Ref
				Large strain	Small strain (< 10%)		
Individual ZnO fine-wire	Piezoelectric	0.2%	1.2%	–	1250	–	1
ZnSnO3 nanowires	Piezoelectric	0.08%	0.32%	–	3740	–	2
P(VDF-TrFE)/Graphene transistor	Piezoelectric	0.008%	0.24%	–	389	–	3
AgNWs/Ecoflex/AgNWs	Capacitive	–	50%	0.7	0.7	~1	4
CNTs/PDMS/CNTs	Capacitive	1%	300%	0.97	0.97	0.9999	5
SWCNTs/Ecoflex/SWCNTs	Capacitive	–	50%	0.41	0.41	0.969	6
Graphene woven fabric	Piezoresistive	2%	6%	–	1000	–	7
Graphene nanosheet composite	Piezoresistive	6%	800%	35	–	–	8
Rubber/MWCNTs/rubber	Piezoresistive	8.3%	620%	43.4	5	–	9
Ag nanowire network	Piezoresistive	–	70%	5	1	0.94	10
CNT percolation network	Piezoresistive	–	1380%	1	~0.1	0.98	11
CNT embroidered graphene	Piezoresistive	1%	20%	–	0.36	–	12
Aligned SWCNTs	Piezoresistive	–	280%	0.06	0.82	–	13
MWCNTs forest/PU Composite	Piezoresistive	–	300%	3.2	0.3	–	14
Microcrack-assisted Ag nanowire network	Piezoresistive	–	60%	150000	–	0.989	15
Carbon nanotube/polydimethylsiloxane composites	Piezoresistive	–	50%	15	1.1	–	16
Vertical CNT-Ecoflex Nanofins	**Piezoresistive**	**0.1%**	**500%**	**8.06**	**6.99**	**0.9952**	**This work**

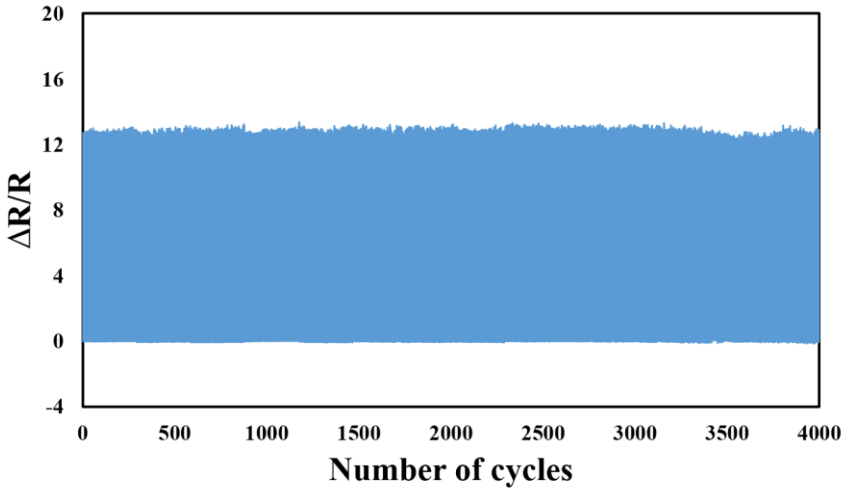

Fig. S2. Repeatability test of the CEN-based strain sensor for the high strain from 0 to 200% for more than 4000 cycles with a strain rate of 40% s^{-1}.

Vertical CNT network model

Since the ends of the vertical CNTs were embedded into the PDMS substrate, the cross-sectional view SEM images of the samples were taken and shown in Fig. S1. To validate the microscopic mechanism of the vertical CNT networks, we carried out a numerical simulation. First, a 2D model of vertical network was generated to describe the cross-section distribution of the CNTs along the stretching direction. There are about 80 nanotubes per micrometer for the sample with a density of 6.44×10^{11} cm^{-2}. The CNTs in the network stand vertically with a tilt angle within the range of 20°. So that, the nanotubes can contact with their neighbors and form enormous conductive paths. Compared with the tube-tube contact resistance, the pristine resistance of the CNTs is negligible. The tube-tube contact conduction of CNTs is believed to be a sort of tunneling effect. The general tunneling resistance between two neighboring CNTs can be given by[17]

$$r_t = \frac{h^2 d}{e^2 A\sqrt{2m_e\varphi}} exp\left(\frac{4\pi d\sqrt{2m_e\varphi}}{h}\right)$$

Where h is the Plank's constant, e is the charge of electron, d is the distance between the two electrons, φ is the height of the energy barrier, m_e is the static mass of the electron, and A is the contact area. The behavior of the vertical CNT network was analyzed by the Monte-Carlo method and the total resistance of the film was calculated by using the Kirchhoff's current law and Ohm's law. To obtain the total resistance change under a specific strain, the positions and orientations of all CNTs were calculated and the connectivity between CNTs was analyzed again.

The distribution of the connected nanotube joints and the morphology of the networks were shown in Fig. S2a. The number and density of the joints decreased at the strain of 100%. The calculated relative change of the resistance for the strains up to 100% by the model is presented in Fig. S2b. As the figure shows, the sample exhibits high sensitivity at both large and small strains.

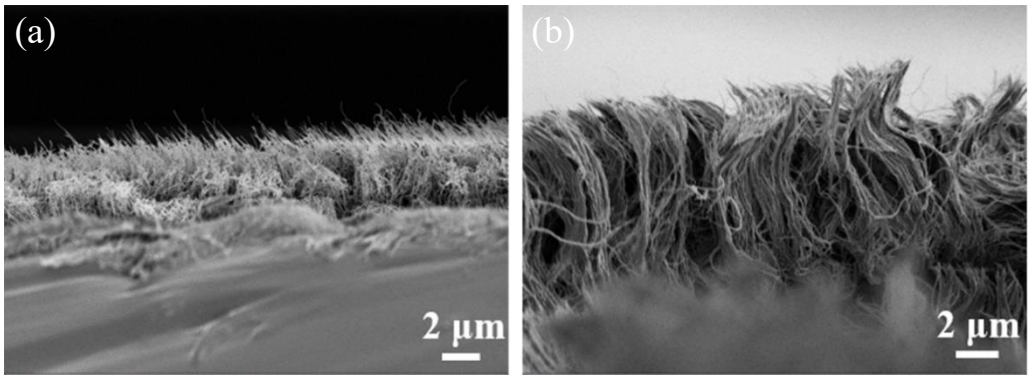

Fig. S3 The SEM images of the transferred vertical CNT networks. (a) The cross-sectional view of the 5 μm CNT network. (b) The cross-sectional view of 50 μm CNT network. Most of the CNTs protrude out from the PDMS. The lengths of the exposed CNTs are about 4 μm and 40 μm for the 5 μm and 50 μm CNT samples, respectively.

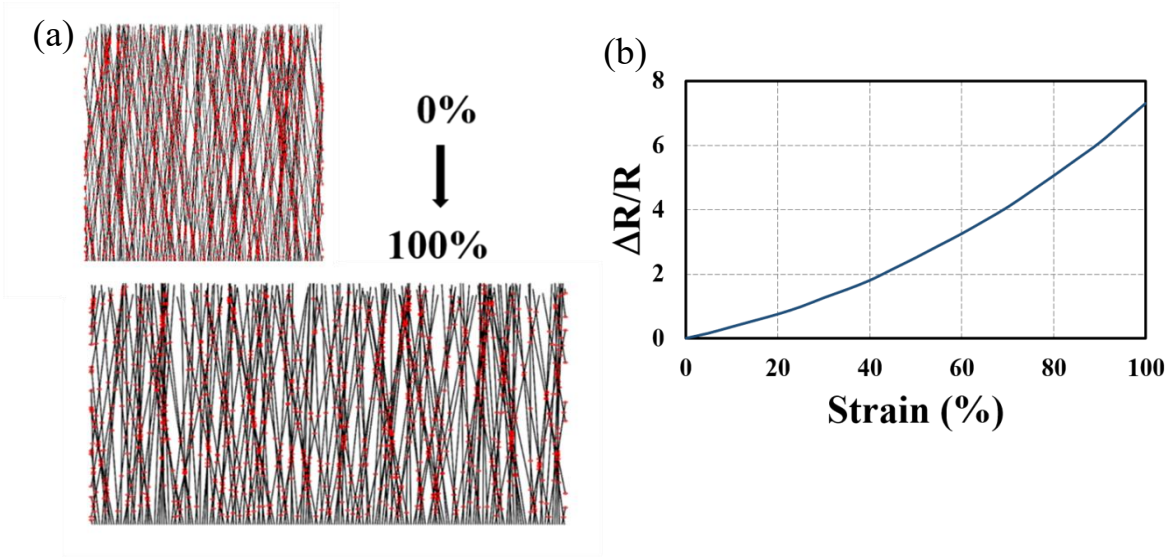

Fig. S4. (a) Projected cross-sectional view of the vertical CNT networks at pristine length and 100% strain. (b) Piezoresistive response for the vertical CNT-based strain sensor obtained by simulation.

Reliability properties of the reinforced vertical CNT networks

As the schematic diagram of the vertical CNTs networks shows in Fig. S3, the vertical nanotubes are controlled by two forces: the interactions between vertical CNTs and the PDMS substrate, and the friction force between the neighboring nanotubes. The strong binding effect between the substrate and the bottom of the vertical CNTs ensures the nanotubes to move with the stretching of the PDMS substrate, resulting in the detachment of part of the adjacent nanotube joints. However, the presence of the friction force prevents the detachment and the recovery of the joints on the stretching/releasing cycles by decreasing the standing angles of the CNTs, leading to low sensitivities and poor reversibility, as shown in Fig. S4.

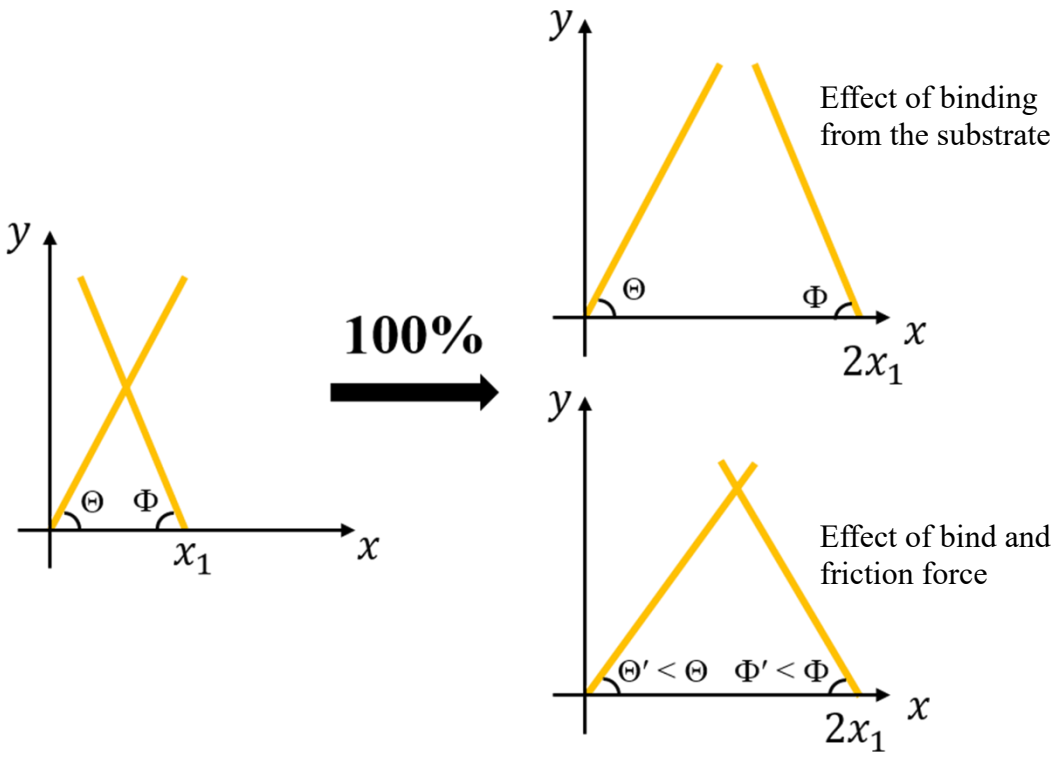

Fig. S5. Schematic diagram of the movements of the CNTs under the effect of the binding between the substrate and CNTs, as well as the friction force between the connected nanotubes at the strain of 100%.

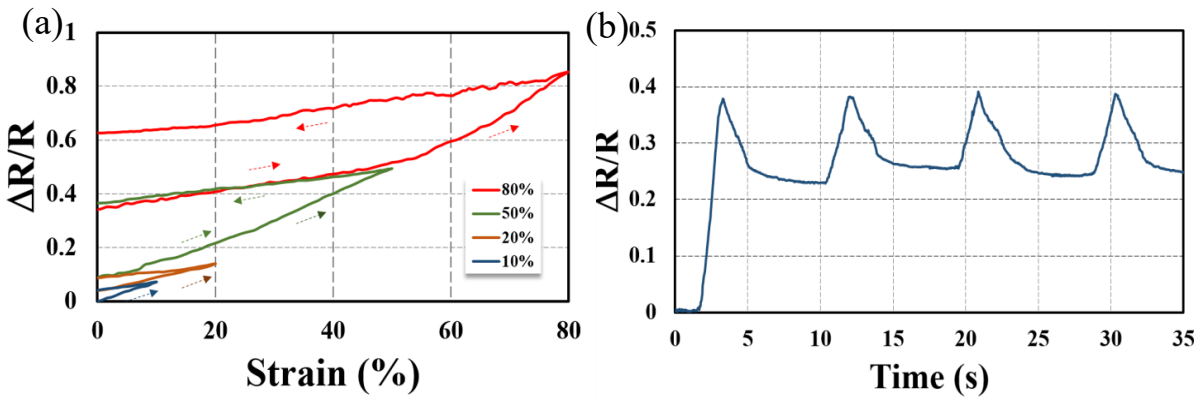

Fig. S6. Effect of the applied strain on the reinforced vertical CNT networks. a) Resistance change versus strain for the sample. The ΔR/R increases when the sample is stretched. However, the resistance cannot fully return to the original value after the strain is released. The resistance continues to increase when strain exceeds the value, at which the strain was released before. The sequence is repeated from 10% to 80%. b) Resistance change versus time in response to cycles of stretching from 0 to 50%. The pristine resistance increases in the first two cycles, and then keeps reproducible.

References

1. J. Zhou, Y. Gu, P. Fei, W. Mai, Y. Gao, R. Yang, G. Bao and Z. L. Wang, *Nano Lett.*, 2008, **8**, 3035-3040.
2. J. M. Wu, C.-Y. Chen, Y. Zhang, K.-H. Chen, Y. Yang, Y. Hu, J.-H. He and Z. L. Wang, *ACS Nano*, 2012, **6**, 4369-4374.
3. Q. Sun, W. Seung, B. J. Kim, S. Seo, S. W. Kim and J. H. Cho, *Adv. Mater.*, 2015, **27**, 3411-3417.
4. S. S. Yao and Y. Zhu, *Nanoscale*, 2014, **6**, 2345-2352.
5. L. Cai, L. Song, P. Luan, Q. Zhang, N. Zhang, Q. Gao, D. Zhao, X. Zhang, M. Tu, F. Yang, W. Zhou, Q. Fan, J. Luo, W. Zhou, P. M. Ajayan and S. Xie, *Sci. Rep.*, 2013, **3**, 3048.
6. D. J. Lipomi, M. Vosgueritchian, B. C. Tee, S. L. Hellstrom, J. A. Lee, C. H. Fox and Z. Bao, *Nat Nanotechnol*, 2011, **6**, 788-792.
7. X. Li, R. J. Zhang, W. J. Yu, K. L. Wang, J. Q. Wei, D. H. Wu, A. Y. Cao, Z. H. Li, Y. Cheng, Q. S. Zheng, R. S. Ruoff and H. W. Zhu, *Sci. Rep.*, 2012, **2**, 6.
8. C. S. Boland, U. Khan, C. Backes, A. O'Neill, J. McCauley, S. Duane, R. Shanker, Y. Liu, I. Jurewicz, A. B. Dalton and J. N. Coleman, *ACS Nano*, 2014, **8**, 8819-8830.
9. S. Tadakaluru, W. Thongsuwan and P. Singjai, *Sensors*, 2014, **14**, 868.
10. M. Amjadi, A. Pichitpajongkit, S. Lee, S. Ryu and I. Park, *ACS Nano*, 2014, **8**, 5154-5163.
11. M. Amjadi, Y. J. Yoon and I. Park, *Nanotechnology*, 2015, **26**, 375501.
12. J. Shi, X. Li, H. Cheng, Z. Liu, L. Zhao, T. Yang, Z. Dai, Z. Cheng, E. Shi, L. Yang, Z. Zhang, A. Cao, H. Zhu and Y. Fang, *Adv. Funct. Mater.*, 2016, **26**, 2078-2084.
13. T. Yamada, Y. Hayamizu, Y. Yamamoto, Y. Yomogida, A. Izadi-Najafabadi, D. N. Futaba and K. Hata, *Nat Nanotechnol*, 2011, **6**, 296-301.
14. M. K. Shin, J. Oh, M. Lima, M. E. Kozlov, S. J. Kim and R. H. Baughman, *Adv. Mater.*, 2010, **22**, 2663-2667.
15. X. Q. Liao, Z. Zhang, Z. Kang, F. F. Gao, Q. L. Liao and Y. Zhang, *Mater. Horiz.*, 2017, **4**, 502-510.
16. Q. Li, J. Li, D. Tran, C. Luo, Y. Gao, C. Yu and F. Xuan, *J. Mater. Chem. C*, 2017, **5**, 11092-11099.
17. J. G. Simmons, *J. Appl. Phys.*, 1963, **34**, 1793-&.